Biomed Microdevices (2007) 9:647–656
DOI 10.1007/s10544-007-9058-2

Surface acoustic wave concentration of particle and bioparticle suspensions

Haiyan Li · James R. Friend · Leslie Y. Yeo

Published online: 26 May 2007

Abstract A rapid particle concentration method in a sessile droplet has been developed using asymmetric surface acoustic wave (SAW) propagation on a substrate upon which the droplet is placed. Due to the asymmetry in the SAW propagation, azimuthal bulk liquid recirculation (acoustic streaming) is generated. Once the local particle concentration is sufficiently high within a particular streamline of the acoustic streaming convective flow, shear-induced migration gives rise to an inward radial force that concentrates the particles at the centre of the droplet. In this paper, a SAW device consists of a 0.75-mm thick, 127.68° *Y*–*X*-axis-rotated cut, *X*-propagating $LiNbO_3$ for a substrate and an interdigital transducer electrode (IDT) with 25 straight finger pairs in a simple repeating pattern, 12 mm aperture, and a wavelength of λ=440 μm was patterned on the substrate. The IDT was then driven with a sinusoidal signal at the resonance frequency f_0 of 8.611 MHz. To investigate the effect of particle type and size on the concentration process, three types of particles were used in this study, including fluorescent particles (1 μm), polystyrene microspheres (3, 6, 20, 45 μm), and living yeast cells (10–20 μm). Different RF powers were applied ranging from 120 to 510 mW. The concentration processes occurs within 2 to 20 s, depending on the particle size, type and input radio frequency (RF) power, much faster than currently available particle concentration mechanisms due to the large convective velocities achieved using the SAW device. Moreover, this concentration method is efficient, concentrating the particles into an aggregate one-tenth the size of the original droplet. Most importantly, bioparticles can also be concentrated by this method; we have verified that yeast cells are not lysed by the SAW radiation during concentration. By using the rapid concentration process described in this work, the breadth of applications and measurement sensitivity of SAW biosensor systems should be greatly enhanced.

Keywords Surface acoustic wave · Particle concentration · Biosensor

H. Li · J. R. Friend (✉) · L. Y. Yeo
Department of Mechanical Engineering,
Micro/Nanophysics Research Laboratory,
Monash University, 133/31 Engineering,
Clayton, Victoria 3800, Australia
e-mail: james.friend@eng.monash.edu

1 Introduction

In the last decade many reports have been published using piezoelectric sensors for a wide range of applications in the food industry, environmental monitoring, clinical diagnostics and biotechnology (Suleiman and Guilbault 1994). Generally, piezoelectric biosensors are based on a coating set upon the surface of the piezoelectric sensor with a selective binding substance, for example, antibodies for bacteria. Once the device is placed in a solution containing bacteria, the bacteria binds to the antibodies, slightly increasing the solid mass of the device, and hence lowering the oscillation resonance frequency, which is proportional to the change in mass. The most prominent devices used are quartz crystal microbalances (QCM) and surface acoustic wave (SAW) resonators (Dickert et al. 2003). However, it takes a substantial amount of time to concentrate the bacteria or other target samples in order to ensure the target sample concentration has reached a detectable value, i.e., before molecular binding may occur (Ivnitski et al. 1999). The capture of particles for detection via a "couple-match" process between the target particles and substrate coating is

enabled solely by diffusion for microdevices. Given that the diffusion time scale, $T_d \sim L^2/D$, where L is the characteristic length scale of the device, typically 10^{-3} m, and $D \sim 10^{-10}$ m^2/s is the species diffusivity, the required diffusion time is measured in hours or even days. In addition, the particles are required to be at or sufficiently close to the substrate before the molecular binding event can take place. Due to these two problems, the detection time will normally be 10 h or longer when using piezoelectric biosensors, prohibitive for many applications (Howe and Harding 2000; Koenig and Gratzel 1993). If it were possible to accelerate the process of capture through agitation of the fluid containing the target particles, and to perhaps concentrate the particles to reduce the diffusion length scale or increase the probability of couple matching, the performance of these biosensors may be dramatically improved.

Concentration of target samples is a generic and widespread fluidic process in biochemical analysis. For dilute samples, an effective collection procedure for targets can significantly reduce the amount of fluid handling (Ho 2001; Wong et al. 2004). In most cases, concentration of targets from the sample can minimize measurement noise and therefore improve detection sensitivity. There are many conventional methods of sample concentration, including filtration, centrifugation, liquid–liquid extraction, and solid-phase adsorption (Belter et al. 1998). Other techniques have also been developed for concentrating target samples in microfluidic chips, such as microfabricated sieving filters (van Rijn et al. 1999), evaporation-based concentration (Walker and Beebe 2002), acoustic radiation pressure (Meng et al. 1999), and electrohydrodynamically driven microcentrifuges (Yeo et al. 2006a,b). Each of these methods are feasible in certain situations but also have disadvantages, principally in fabrication complexity, processing delays, and difficulty in integration with other fluidic components. A physical force field that could concentrate targets on an activated sensor surface without such limitations would be attractive for some applications.

Acoustic forces can be used to noninvasively position, concentrate, or fractionate particles. One method uses a high frequency travelling wave together with acoustically driven bulk internal convection, known as acoustic streaming, while another employs low frequency flexural standing waves in a plate (Bennès et al. 2006). Kundt and Lehmann (1874) first described the use of acoustic standing waves to concentrate initially homogeneously suspended particles at acoustic pressure nodal or antinodal planes in a fluid. Recently, Hawkes et al. (2004) used ultrasonic standing waves to deposit cells on a surface. Yasuda et al. (1996) also applied an ultrasonic standing plane wave to concentrate small particles. In the presence of an ultrasonic standing wave, suspended particles in the liquid experienced radiation forces that drove them towards pressure nodes or antinodes. The nodes or antinodes were planar rather than at a single point or among a group of points. For bioparticle concentration, the target particles were dispersed in highly dilute solutions, and the concentration of analytes along a plane in the fluid would not necessarily improve the detection sensitivity of a biosensor. Moreover, it still takes several minutes for particle collection in these devices.

Recently, SAW technology has also been applied to microscale fluid actuation and micro-mixing (Sritharan et al. 2006; Wixforth et al. 2004; Guttenberg et al. 2004). Wixforth (2004) has demonstrated that SAWs interact very efficiently with small liquid droplets located along the surface of a piezoelectric substrate. They also discussed the basic droplet manipulation mechanism via acoustic streaming, depicted in Fig. 1(a). A surface acoustic wave may be efficiently generated on a piezoelectric substrate using a metallic coating patterned into an interdigital transducer electrode (IDT) as shown in Fig. 1(b). The SAW travels along the substrate from left to right. Once the SAW reaches the droplet, the acoustic radiation is *leaked* into the fluid, which in turn induces acoustic streaming in the fluid (Sritharan et al. 2006). The SAW propagating along the substrate entering the droplet is diffracted under an angle θ_R into the fluid, where it generates a longitudinal pressure wave. For an infinite half space, this diffraction angle is given by the ratio of the sound velocities of the SAW along the substrate and the bulk longitudinal wave in the fluid, respectively. If the intensity of the acoustic radiation component into the fluid is sufficiently high and the liquid consists of a free droplet whose contact line is not pinned, the SAW can induce the droplet to translate in the direction of the SAW. We will, however, consider the case where the acoustic intensity is lower than the threshold required to translate the drop. In these cases, only bulk liquid recirculation is observed within the drop, even though its contact line may not be pinned. Figure 1(a) also illustrates the attenuation and eventual extinction of the SAW in the substrate. For smaller droplets and higher input powers, the SAW may continue past the droplet in the substrate at a reduced amplitude.

A key to concentration of material within a droplet is an asymmetric distribution of SAW radiation along the width of the droplet and transverse to the radiation propagation direction. There are many ways to achieve this situation; Fig. 1(b) illustrates three approaches. By placing the droplet along one side of the radiation propagating from the IDT, either with or without a reflector, the droplet encounters acoustic radiation over a fraction of its width. Another way is to control the SAW radiation reflected from the side opposite the input IDT by shielding off one half of an open reflector on the other end of the device using a damping material (viz. α-gel, Oba Machinery Ltd., Shizuoka, Japan)

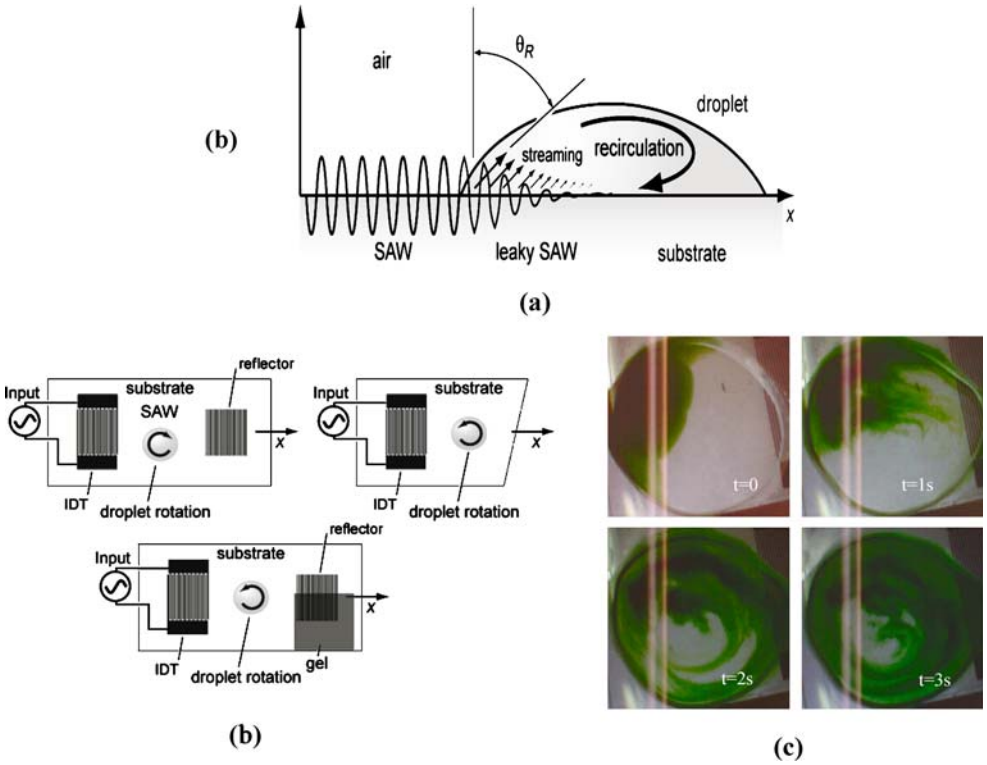

Fig. 1 (**a**) Sketch of the acoustic streaming acting on a small droplet on the SAW surface. The acoustic energy is radiated into the fluid under an angle θ_R, leading to internal streaming in the small fluid volume. (**b**) Schemes for symmetry breaking of SAW propagation in order to generate azimuthal liquid recirculation. The left pictures shows one of the IDTs partly covered with α-gel damping material and the right picture shows the use of only one IDT with the wafer cut in a diagonal fashion. (**c**) Images at 60 frames/s showing the visualisation of azimuthal bulk recirculation generated by asymmetric SAW propagation through dye streamlines induced by the flow

to form standing-wave and traveling-wave SAW across the width of the droplet. A simpler way is to cut the edge opposite the input IDT at an angle to the propagation axis to reflect the SAW radiation at an angle. This method has been experimentally verified to form azimuthal flow within the drop as shown in Fig. 1(c). Since SAW is shallow, at around four to five wavelengths deep, it is not necessary to cut through the wafer. Shallow channels etched into the surface of the substrate would be sufficient to reflect the radiation. It is also possible to design the IDTs to form the desired asymmetric radiation pattern, though this is beyond the scope of this paper.

Here, we focus on the curious phenomenon that particles suspended in the liquid droplet are rapidly convected and hence aggregate at the centre of the droplet within approximately 15 s. In this paper, we demonstrate SAW-induced azimuthal acoustic streaming for microfluidic particle concentration as a means to overcome diffusion limitations in the couple-matching and concentration process such that the sensitivity of biosensors may be enhanced. To our knowledge, there is no current method for particle trapping or concentration from bulk suspension at these speeds.

Fluorescent particles were used to monitor the concentration process via fluorescence microscopy. The concentration process was recorded via high-speed video, and the quality and speed of concentration was determined using centre-normalized pixel intensity analysis (NPI) of individual image frames extracted from the video. Different RF powers were used to study its effect on the concentration process and the effect of particle size was also investigated. Living yeast cells were used to demonstrate the concentration of bioparticles. The viability of the cells was investigated using methylene violet stain which only penetrates dead yeast cells.

2 Experimental materials and method

2.1 Materials

Fluoresbrite® multifluorescent polystyrene (PS) microspheres (Polysciences, Inc., USA), 1 μm in diameter and with an initial concentration of 4.55×10^{10} particles/ml were used. Using deionized (DI) water, the original suspension was diluted to obtain a concentration of 4.55×10^{8} particles/ml. The dilute solution was dispersed using ultrasound and stirred by pipette before being dispensed onto the device substrate. The particles were dyed with three different fluorescent dyes with absorption maxima at 377, 517 and 588 nm, and excitation maxima at 479, 546 and 612 nm, respectively.

Plain PS microspheres, with diameters 3, 10, 20 and 45 μm (Polysciences, Inc., USA), were also used to study the effect of particle size on the behaviour of the SAW device. The suspension concentrations for the 3, 10, 20 and 45 μm particles were 1.68×10^{9}, 4.55×10^{7}, 5.68×10^{6} and 4.99×10^{5} particles/ml, respectively. DI water was used to

adjust the four suspensions to a sample concentration of 4.99×10^5 particles/ml.

Stock cultures of the yeast cells were maintained on standard agar consisting of 1% yeast extract, 0.5% neutralized bacteriological peptone, and 1% glucose solidified with 1.5% agar (w/v). All media were autoclaved immediately after preparation at 121°C and 15 psi for 15 min. Yeast cells were grown aerobically to the required cell density at room temperature.

2.2 Method

A SAW can be excited by the application of a radio frequency signal to an IDT on a piezoelectric substrate. The wavelength of the excited SAW is defined by the geometry of the IDT. In this experiment, the SAW device consists of a 0.75-mm thick, 127.68° *Y*–*X*-axis-rotated cut, *X*-propagating $LiNbO_3$ (Lithium Niobate or LN, Roditi, London UK) single crystal substrate to generate Rayleigh waves, a SAW comprised of coupled vibration along the propagation axis and perpendicular to the substrate plane (White and Voltmer 1965). The IDT consists of 25 straight finger pairs in a simple repeating pattern, a 12 mm aperture, and a wavelength of λ=440 μm which defines the strip and gap widths to be 110 μm. The IDT was driven with a sinusoidal signal at the resonance frequency f_0, defined as $f_0=c/\lambda$. The SAW velocity c=3788 m/s, and hence $f_0\approx8.611$ MHz. Such an IDT efficiently converts the applied RF signal into an acoustic wave, which in this case travels with little divergence from the IDT in both directions perpendicular to the direction of the strip electrodes. The droplet was deposited directly on the LN surface, which is mildly hydrophyllic. No droplet translation was induced from acoustic streaming since the input RF power was below the threshold defined by the power necessary to release the contact line pinning present at the edge of the droplet. The drop therefore remained stationary.

Figure 2 is a schematic of the setup as seen from above. Situated on the left side is the input interdigital transducer as connected to an RF power source. A 5-μl sample droplet was then deposited on the surface of the SAW device. Lithium niobate is transparent, and with the rough polish on the underside of the substrate, it was possible to illuminate the droplet from below and use a high-speed video camera (Olympus *i*Speed, Tokyo, Japan) to monitor the motion of the plain PS particles inside the droplet from above. To observe the fluorescent PS particles, a reflection fluorescent stereomicroscope (Olympus BXFM, Tokyo, Japan) has been used. The BXFM fluorescent stereomicroscope has an EXFO X-Cite 120 mercury light source and the heart of the X-Cite 120 is a proprietary 120-W short arc lamp (Olympus, Tokyo, Japan). Wideband blue light was applied to excite the fluorescent particles and a fluorescence mirror unit (U-MWB2) with a DM500 dichroic mirror and the excitation filter and barrier filter are 460–490 nm and BA520IF, respectively.

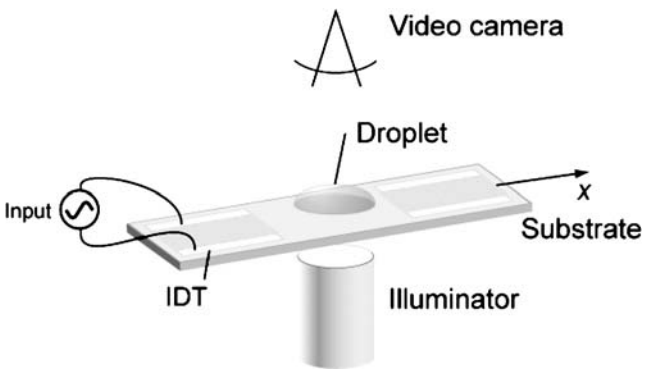

Fig. 2 Schematic representation of the SAW device upon which the liquid test sample is placed

The viability of living yeast cells after concentration was confirmed using a vitality dye, a common method (Smart et al. 1999). Viable yeast cells do not stain, whereas non-viable, non-metabolizing cells stain the colour of the selected dye. In this work, methylene violet 3 RAX (Sigma Chemical Co., USA) was used as the dye and the stain process was performed as described by Smart et al. (1999). Briefly, methylene violet 3 RAX was dissolved in sodium citrate solution (2% w/v) to a final concentration of 0.01% (w/v). The yeast suspension (0.5 ml of 1×10^7 cells/ml suspension) was stirred into 0.5 ml of citrate methylene violet 3 RAX and examined microscopically after 5 min; unstained cells were assumed to be viable.

Individual images extracted from the high speed videos acquired during the concentration process were post-processed by VirtualDub (http://www.virtualdub.com) and Photoshop CS (Adobe Systems Software Ltd, Ireland). The high speed videos were captured at a speed of 60 frames per second, and the exposure time of the camera is therefore 0.017 s since the shutter is 1×. The normalized pixel intensity (NPI) was recorded for quantifying the concentration process. The pixel intensities of the images were acquired using Photoshop CS and each experiment set was repeated three times. The results averaged from each of these datasets were then normalised to the results obtained using the first image at time t=0. Acoustic streaming velocities and the particle velocities were estimated using Diatrack 3.01 (Semasopht, North Epping, Australia).

3 Results

Figure 3(a) shows the behaviour of 1-μm fluorescent PS particles as they are convected within the bulk of the drop by SAW-induced acoustic streaming as individual image frames acquired by high speed fluorescent microscopy at

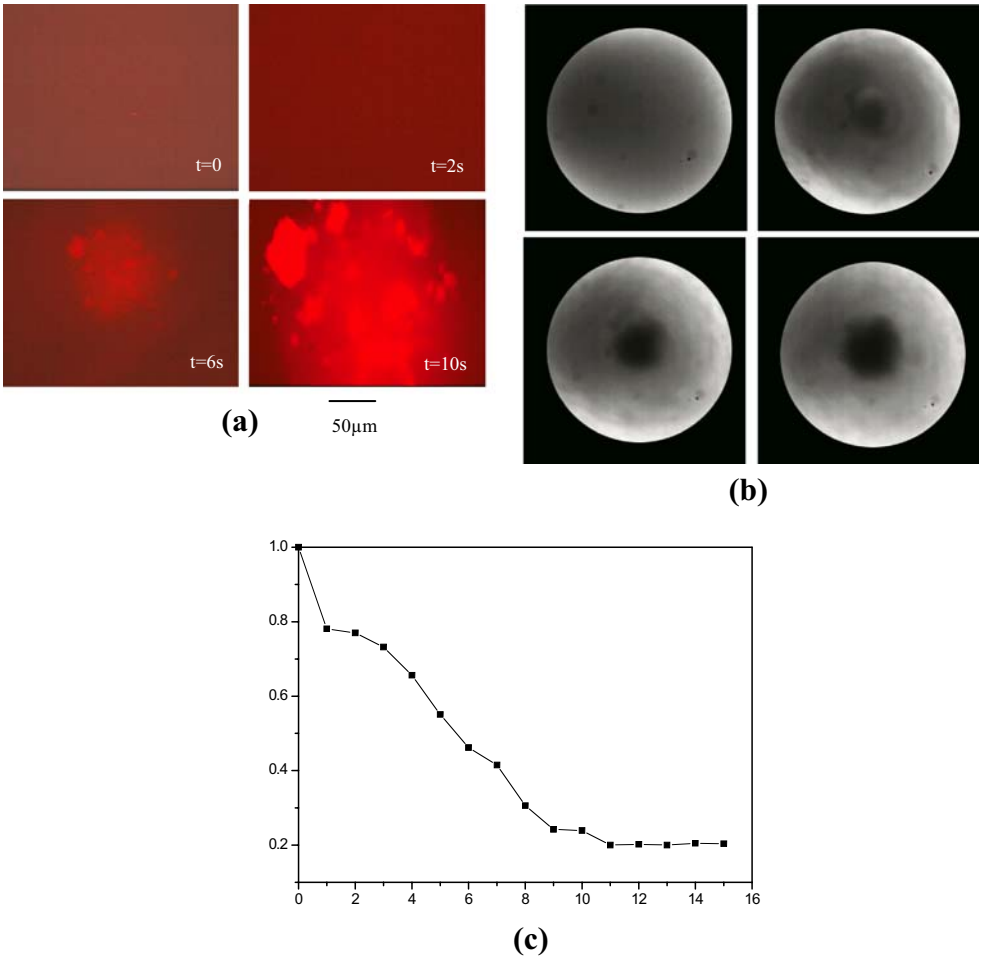

Fig. 3 (**a**) Fluorescent microscopy images acquired at 60 fps, showing early aggregation of initially dispersed 1-μm spherical fluorescent PS particles at the centre of the liquid droplet. (**b**) Bright-field images acquired at 60 fps, showing the rapid concentration of the 1-μm spherical PS fluorescent particles. The RF power is 330 mW in both cases. The area external to the drop in the images was masked to avoid affecting the NPI analysis. (**c**) NPI as a function of time. In all experiments, the particle concentration is 10^8 particles/ml and the input RF power is 330 mW

60 fps. The fluorescence signal, as depicted by the bright spot at the centre of the image and corresponding to the centre of the sample, is observed to grow in intensity and to spread radially outward from the centre as the initially dispersed fluorescent particles appear to concentrate at the centre of the drop.

We observed the NPI to decrease rapidly toward an asymptotic value of 0.2 in just 10 s, indicating the centre particle concentration process is extremely rapid. Figure 3(b) shows a demagnified view of the particle concentration process under whole bright-field illumination, verifying the accumulation takes place in the centre of the drop. Here, we define the time taken for concentration as the period over which the NPI decreases from a value of 1 to a constant value (0.2 in this case). The particle concentration process can be quantified through an NPI analysis, as shown in Fig. 3(c).

The concentration rate is dependent on the RF power input to the IDT and hence the amplitude of the SAW. We observed in Fig. 4(a) that the rate of particle concentration, as described the temporal variation in the NPI, is enhanced as the input power is increased to a critical value of approximately 300 mW. Beyond this point, the concentration efficiency begins to decrease, and there is a sharp decrease upon passing about 500 mW. At these power levels there is virtually no particle concentration, similar to the situation when low input power (<120 mW) is used. These trends are illustrated in Fig. 4(b) where the NPI at t=10 s, which corresponds to the fastest concentration time, is plotted as a function of the input power.

The decrease in particle concentration at high power is attributed to the redispersion of the aggregated particles. Figure 5 represents such a situation; the input power is abruptly increased from a near optimal value of 330 to 510 mW at t=15 s when the particles have become concentrated. The concentrated particles are subsequently dispersed in approximately the same amount of time, 15 s, as shown in the image sequences in Fig. 5(a), and verified by the NPI analysis in Fig. 5(b). There is an initial sharp increase in the NPI due to the abrupt power surge followed by a gradual increase. The particle dispersion at high input power is associated with large acoustic streaming velocities which oppose the dominant particle aggregation mechanism which shall be discussed in the next section. At low power,

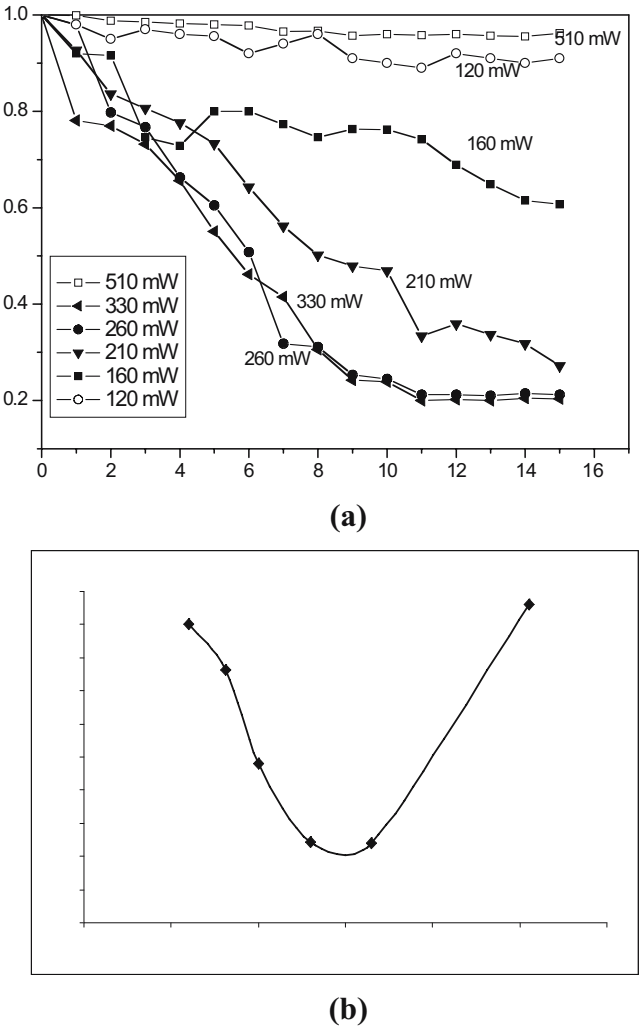

Fig. 4 (**a**) Effect of input RF power on particle concentration variation in the NPI as a function of time, and (**b**) NPI for various powers at time t=10 s. In all experiments, the particle concentration is 10^8 particles/ml wherein 1-μm spherical fluorescent PS particles are utilized

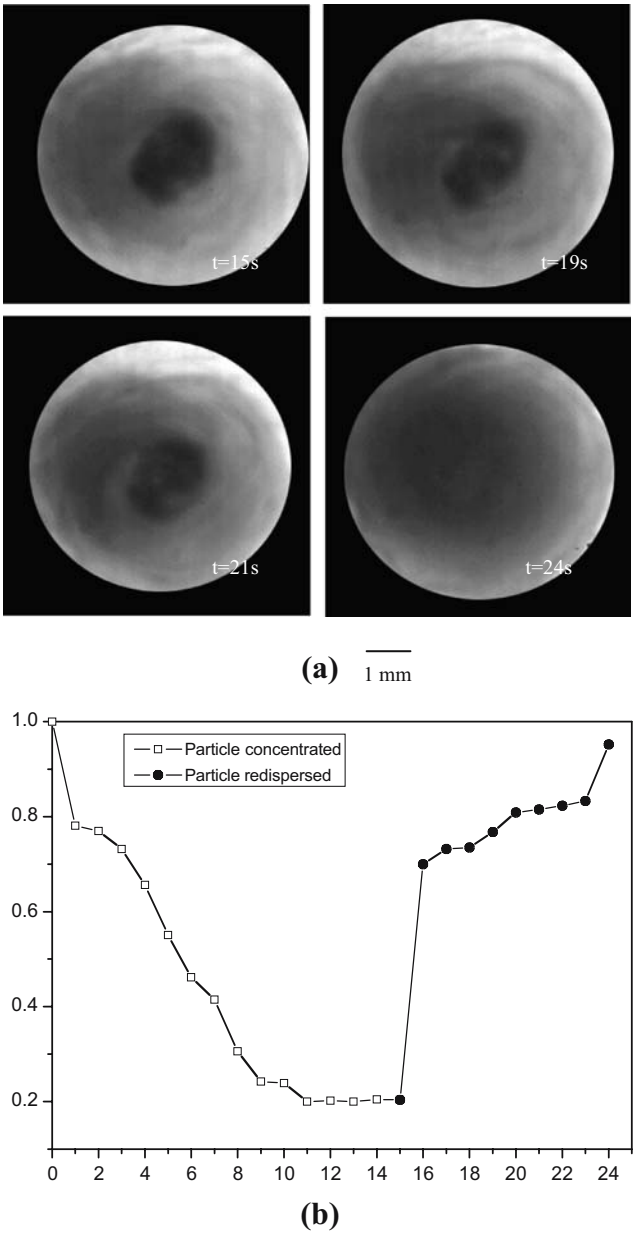

Fig. 5 (**a**) Particle concentration and redispersion through an abrupt increase in the input power after 15 s from 330 to 510 mW. (**b**) NPI analysis. The open data points are the data for an input power of 310 mW concentration of PS microspheress in which is observed and the solid data points represent the 510 mW data where the concentrated microspheres were redispersed. 1-μm fluorescent PS microspheres were used and the initial particle concentration is 10^8 particles/ml

the behaviour is similar, but the reason is entirely different: the convection velocity is insufficient to drive particle aggregation.

The concentration rate increases as the particles become larger as shown in Fig. 6. It can be seen that only 2 s is required for the concentration of 45 μm PS microspheres in Fig. 6(a). This increased to approximately 15 s for the smallest particle size in our test sample, i.e. 10 μm. The size effect can be more clearly seen in Fig. 6(b), where we observe the concentration time to scale as $1/a^2$, where a is the particle dimension. This has important implications in identifying the concentration mechanism as will be discussed in the next section. Curiously, the concentration time for 3-μm particles does not fit the $1/a^2$ trend. This may be due to cluster formation prior to final concentration, which can be seen in the images acquired under fluorescence (Fig. 3), indicating the fluorescent particles aggregate into larger particulate masses before moving to the centre. The surface area is large for such small particles, increasing the likelihood that the observed aggregation is due to van der Waals forces. Upon clustering, the effective particle size a becomes the cluster size, leading to a tenfold decrease in the concentration time.

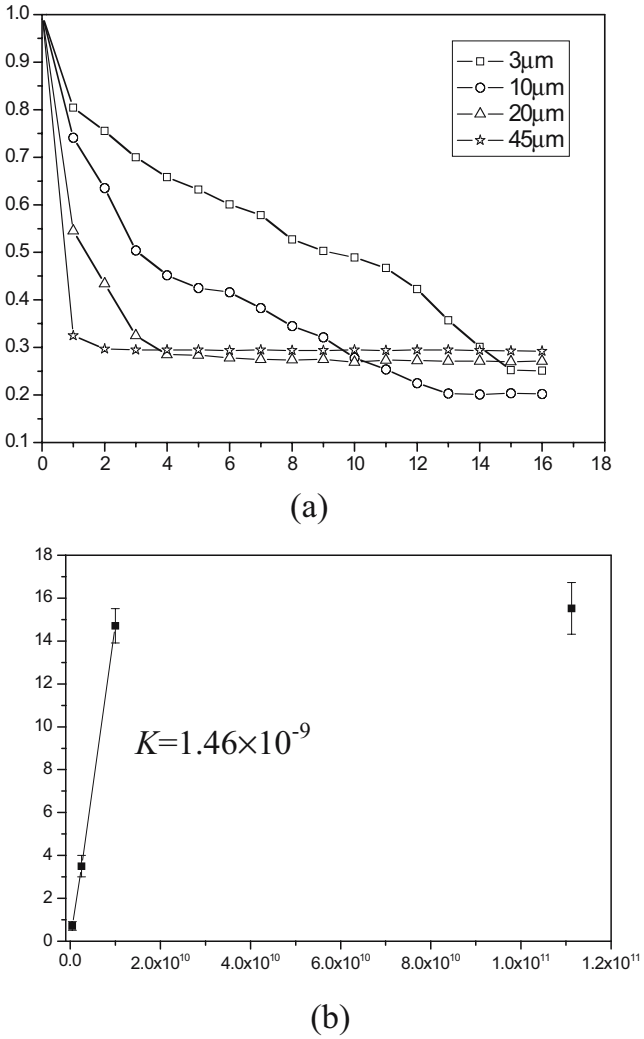

Fig. 6 (**a**) Size dependence of the particle concentration process. NPI as a function of time. (**b**) Time for particle concentration. The particles used in this dataset are plain PS microspheres with an initial particle concentration of 10^5 particles/ml. The RF power is held constant at 330 mW

Living yeast cells were used to determine the effect of the SAW concentration process on bioparticles. Before concentration, the cell sample was stained with methylene violet to confirm that they were alive. The yeast cell suspension was mixed with dye solution and the mixture immediately pipetted onto the SAW substrate. The whole concentration process was carried out at an RF input power of 330 mW giving the results as shown in Fig. 7. As with the synthetic particles, the initially dispersed yeast cells (Fig. 7(a)) rapidly concentrated at the centre of the drop (Fig. 7(b) and (c)). To investigate the effect of the SAW energy on the viability of the living yeast cells, the concentrated cells were withdrawn by pipette, remixed with dye solution and examined under a microscope after 5 minutes. Figure 8(a) shows images of living yeast cells prior to the concentration process. The cells are nearly

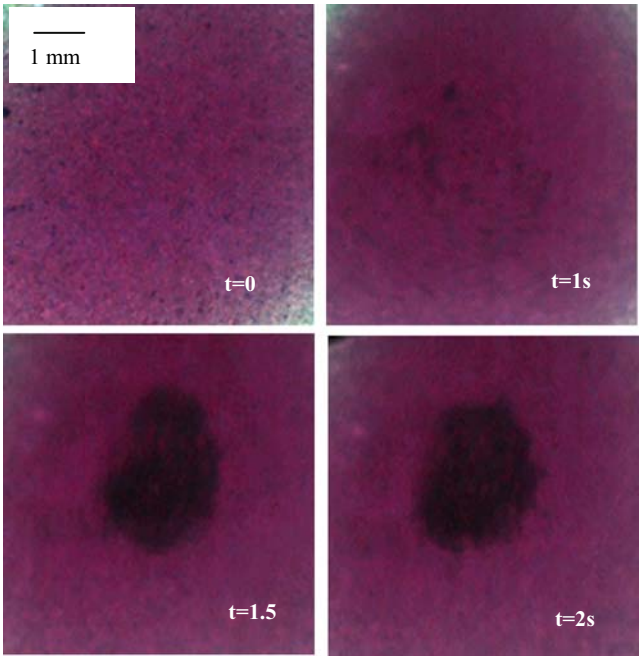

Fig. 7 Sequences of image acquired at 60 frames/s showing the concentration of living yeast cells. The RF input power is 330 mW and the initial yeast concentration is 1×10^7 particles/ml. The yeast size ranges from 5 to 10 μm and most of them are oval in shape

transparent, indicating that the yeast cells were alive before the start of the SAW concentration process. We verified that the large black spots dispersed in the fluid in Fig. 8 were found only in the suspension of living cells; it is thus possible to attribute these as the *pseudohypha* (elongated

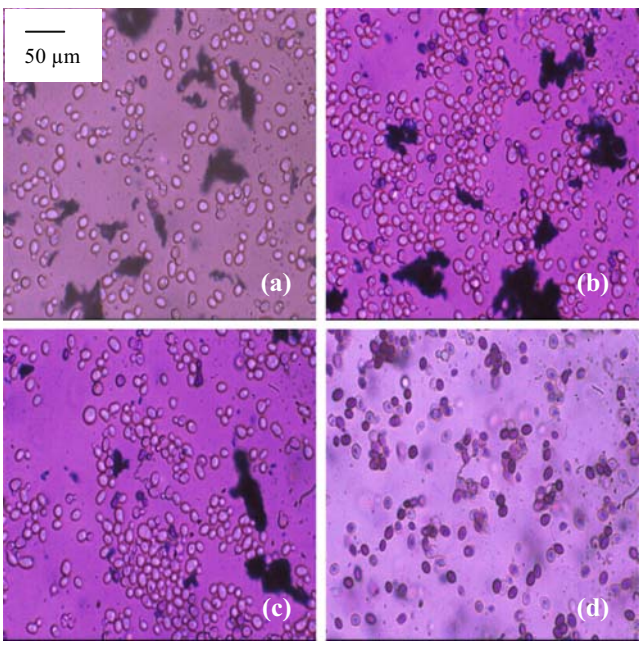

Fig. 8 Microscopic images of living yeast cells stained by methylene violet before (**a**) and after concentration (**b**–**c**); (**d**) stained dead yeast cells. The yeast size ranges from 5 to 10 μm and most of them are oval in shape

cells) produced during the live yeast cells' proliferation. Figure 8(b) and (c) show the state of the cells within the droplet after the concentration process. The yeast cells are still transparent after a subsequent stain, indicating that the cells' viability was not affected by the SAW radiation. For comparison, stained dead yeast cells are shown in Fig. 8(d), where the difference is quite clear: the dead cells are stained purple in contrast to those in Fig. 8(a), (b) and (c).

We now turn to postulate the mechanism by which the particle concentration and dispersion occurs. The $1/a^2$ particle size dependence on the concentration time, as observed in Fig. 6(b), strongly suggests that shear-induced migration plays an important role in the concentration process. If it can be assumed that the azimuthal liquid recirculation due to the asymmetry in the SAW wave propagation across the transverse direction of the droplet (Fig. 2) gives rise to constant angular rotation with speed ω, then the azimuthal velocity $V_\theta = r\omega$, where r is the radial coordinate, must decrease linearly from the outer radius of the droplet $r=R$ to the centre of the drop $r=0$. Thus, particles on the outer periphery of the drop are induced to diffuse from this high shear region towards the low shear region in the centre of the droplet, thus leading to particle concentration at the centre of the droplet.

The diffusion time for shear-induced migration into a vortex of radius R is

$$T_{\mathrm{sm}} \cong \frac{R^2}{a^2\gamma\varphi} \tag{1}$$

where γ is the shear rate and ϕ is the local particle volume fraction in the vortex, which can be taken to be the hard sphere maximum packing fraction, i.e. $\phi=0.68$. The agreement with the inverse particle dependence therefore

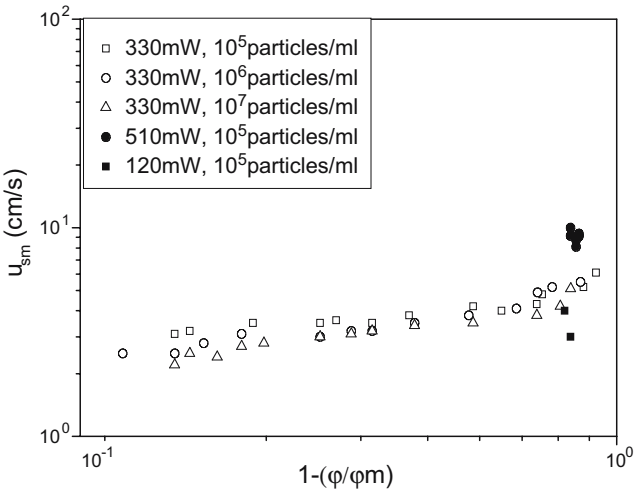

Fig. 9 Shear-induced migration velocities (u_{sm}) as a function of ϕ for a suspension of 10-μm plain PS particles in DI water

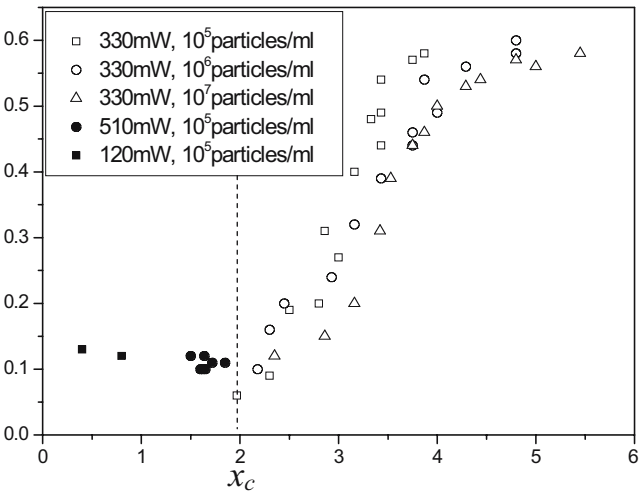

Fig. 10 Change in vortex particle vortex volume fraction ö versus the ratio between the acoustic streaming velocities (u_{as}) and shear-induced migration velocities (u_{sm}) χ for a suspension of 10-μm polystyrene particles in DI water. The open data points indicate that the particles are concentrated and the solid data points indicate that the particles are dispersed

lends support to this postulated mechanism, at least for 10 μm particles and larger in the experimental data in Fig. 6(b). Furthermore, we verify that the slope in Fig. 6(b), 1.46×10^{-9}, is roughly of the same order as $R^2/\gamma\phi \sim 10^{-9}$ m^2 s from Eq. 1; from our images $R\sim10^{-3}$ m and $\gamma\sim10^{3}$ s^{-1} from the particle mean velocities measured with the use of particle tracking software. The shear-induced diffusion time to achieve the maximum hard sphere packing fraction $\phi_{\mathrm{m}}=0.68$ given by Eq. 1, approximately 10 s, agrees well with the magnitude of the time required for particle concentration obtained in the experiments.

We also observe the reduction in the vortex size in which the particles are concentrated (spot size in Figs. 3, 5 and 7) as ϕ increases. This is associated with a decrease in the particle convective velocity (u), as shown in Fig. 9. For the solid round points, the convection is so strong that it overcomes shear-induced migration and leads to redispersion of the particles. This will be discussed subsequently. The solid square points correspond to the condition where there is insufficient convection to cause initial particle concentration along a streamline which begins the process of shear-induced migration. Thus, there is no particle concentration, as discussed previously.

The redispersion of the aggregated particles at high acoustic powers is attributed to the presence of strong internal bulk convection. While a certain amount of internal convection or recirculation is necessary to convect the particles into a streamline to begin shear-induced migration, excessive acoustic streaming-induced convection velocities can overwhelm the shear-induced migration process. The competition between bulk acoustic convection (acoustic

streaming) and shear-induced migration can be quantified by the parameter

$$\chi \equiv \frac{u_{as}}{u_{sm}}, \tag{2}$$

where

$$u_{as} = \frac{PR^2}{7.11 c\mu A l} \tag{3}$$

is the acoustic streaming velocity (Rife et al. 2000), and u_{sm} is the convective particle velocity (u) obtained by using particle tracking software. Further, P is the acoustic streaming power, A is the area across which the power is applied, c is the acoustic velocity in the fluid, l is the acoustic absorption length in the fluid and μ is the fluid viscosity. Figure 10 shows that above a critical value $\chi \sim 2$, shear-induced migration dominates and causes particle concentration. Below this critical value, the bulk internal convection dominates over shear-induced migration and so no particle concentration may take place. This explains why particle concentration does not occur at high input powers. The critical χ value also explains the observation of particle redispersion when the input power is abruptly increased, as shown in Fig. 5. At input powers beyond the critical value (i.e., below $\chi \approx 2$), the outwardly directed centripetal acceleration due to the azimuthal acoustic streaming convection is far larger than the inwardly directed centripetal acceleration due to shear-induced migration.

Finally, the difference between the concentration of synthetic particles and bioparticles is worth mentioning. For particles with a size comparable to the yeast cells (typically 10–20 μm), the concentration time is approximately 15 s in contrast to yeast which requires only about 2 s. A possible reason for this is the formation of clusters of the bioparticles similar to that discussed previously for the small 3 μm particles where the observed concentration time is much smaller than that predicted by Eq. 1. This is because the effective size of the particle cluster should replace the particle size a in the equation, thus giving a smaller diffusion time for shear-induced migration. Further, bioparticles yeast cells are typically much more deformable (Ahimou et al. 2003) than rigid PS particles and hence the maximum packing fraction would be larger than that for the hard sphere maximum packing fraction of 0.68, shortening the diffusion and hence concentration time.

4 Conclusions

We have demonstrated the rapid concentration of particles in a sessile droplet in 2–20 s by inducing azimuthal bulk liquid recirculation acoustic streaming within the droplet with the use of SAW radiation on the substrate upon which the droplet is placed. A key to inducing azimuthal recirculation is an asymmetry in the SAW radiation across the width of the droplet. Once a sufficient initial local particle concentration is attained along the azimuthal streamline generated by acoustic streaming, shear-induced migration dominates, giving rise to an inward radial force that concentrates the particles at the centre of the droplet. Redispersion of the particle aggregate can also be achieved by increasing the input power such that the bulk internal convection dominates over shear-induced migration such that the outwardly directed centripetal acceleration overcomes the shear-induced diffusion process. The particle concentration process in this technology is faster than currently available particle concentration mechanisms due to the large convective velocities achieved using the SAW device. Moreover, the concentration process is also efficient, concentrating the particles into an aggregate about 10% of the size of the droplet. It was also verified that bioparticles concentrated using this process were not damaged by the SAW radiation. These findings indicate that the limitations of current biosensors can be resolved with the use of the proposed SAW concentration device. The analyte detection sensitivity can thus be increased due to the particle concentration process allowing a wider range of sensor technologies to be used. Moreover, the rapid concentration process reduces the diffusion limitation to the molecular binding couple-matching process as well as the total concentration and detection time. It is thus believed that these advantages will economically improve biosensor technology by using these SAW techniques.

Acknowledgments The authors are grateful to Dr. Christopher Ticknor for imaging the acoustic streaming recirculation in Fig. 1(c). The authors would also like to thank Dr. Christopher Langendorf for providing the yeast cells.

References

F. Ahimou, A. Touhami, Y.F. Dufrene, Yeast **20**, 25 (2003)
P.A. Belter, E.L. Cussler, W.-S. Hu, *Bioseparation: Downstream Processing for Biotechnology* (Wiley, New York, 1998)
J. Bennès, S. Alzuaga, P. Chabé, G. Morain, F. Chérioux, J.-F. Manceau, F. Bastien, Action of low frequency vibration on liquid droplets and particles. Ultrasonics **44**, e497–e502 (Supplement 1, 22 December 2006)
F.L. Dickert, P. Lieberzeit, O. Hayden, Anal. Bioanal. Chem. **377**, 540 (2003)
A. Guttenberg, A. Rathgeber, S. Keller, J.O. Radler, A. Wixforth, M. Kostur, M. Schindler, P. Talkner, Phys. Rev., E **70**, 056311 (2004)
J.J. Hawkes, M.J. Long, W.T. Coakley, M.B. McDonnell, Biosens. Bioelectron. **19**, 1021 (2004)
C.-M. Ho, in *Proc. IEEE MEMS'01* (Interlaken, Switzerland, 2001), p. 375
E. Howe, G. Harding, Biosens. Bioelectron. **15**, 641 (2000)
D. Ivnitski, I. Abdel-Hamid, P. Atanasov, E. Wilkins, Biosens. Bioelectron. **14**, 599 (1999)
B. Koenig, M. Gratzel, Anal. Lett. **8**, 1567 (1993)

A. Kundt, O. Lehmann, Ann. Phys. **153**, 1 (1874)
A.H. Meng, A.W. Wang, R.M. White, in *Proc. Transducers'99 Conference* (Sendai, Japan, 1999), p. 876
J.C. Rife, M.I. Bell, J.S. Horwitz, M.N. Kabler, R.C.Y. Auyeung, W.J. Kim, Sens. Actuators **86**, 135 (2000)
K.A. Smart, K.M. Chambers, I. Lambert, C. Jenkins, J. Am. Soc. Brew. Chem. **57**, 18 (1999)
K. Sritharan, C.J. Strobl, M.F. Schneider, A. Wixforth, Appl. Phys. Lett. **88**, 054102 (2006)
A.A. Suleiman, G.G. Guilbault, Analyst **119**, 2279 (1994)
C.J.M. van Rijn, W. Nijdam, S. Kuiper, G.J. Veldhuis, H. van Wolferen, M. J. Elwenspoek, J. Micromechanics Microengineering **9**, 170 (1999)
G.M. Walker, D.J. Beebe, Lab Chip **2**, 57–61 (2002)
R.M. White, F.W. Voltmer, Appl. Phys. Lett. **7**, 314 (1965)
A. Wixforth, Superlattices Microstruct. **33**, 389 (2004)
A. Wixforth, C. Strobl, Ch. Gauer, A. Toegl, J. Scriba, A.V. Guttenberg, Anal. Bioanal. Chem. **379**, 982 (2004)
P.K. Wong, C. Chen, T. Wang, C.-M. Ho, Anal. Chem. **76**, 6908 (2004)
K. Yasuda, S. Umemura, K. Takeda, J. Acoust. Soc. Am. **99**, 1965 (1996)
L.Y. Yeo, D. Hou, S. Maheshswari, H.-C. Chang, Appl. Phys. Lett. **88**, 233512 (2006a)
L.Y. Yeo, J.R. Friend, D.R. Arifin, Appl. Phys. Lett. **89**, 103516 (2006b)